PHYSICAL REVIEW D VOLUME 51, NUMBER 3 1 FEBRUARY 1995

Hadronic $Z\gamma$ production with QCD corrections and leptonic decays

J. Ohnemus
Department of Physics, University of California, Davis, California 95616
(Received 21 July 1994)

The process $p\overset{(-)}{p} \to Z\gamma + X \to \ell^-\ell^+\gamma + X$, where ℓ denotes a lepton, is calculated to $O(\alpha_s)$. Total and differential cross sections, with acceptance cuts imposed on the leptons and photon, are given for the Fermilab Tevatron and CERN LHC center-of-mass energies. In general, invariant mass and angular distributions are simply scaled up in magnitude by the QCD radiative corrections, whereas in transverse momentum distributions, the QCD radiative corrections increase with the transverse momentum.

PACS number(s): 13.85.Qk, 12.38.Bx, 13.38.Dg, 14.70.−e

I. INTRODUCTION

Measurements of weak boson pair production at hadron colliders are vital for testing the standard model and probing beyond it. These processes are particularly important because they can be used to probe the electroweak symmetry-breaking mechanism and test the triple weak boson couplings [1]. The process $p\overset{(-)}{p} \to Z\gamma$ is of interest as a test of the standard model. In addition, this process is sensitive to contact interactions which appear in composite models of gauge bosons [2], and it can also be used to search for evidence of anomalous $ZZ\gamma$ and $Z\gamma\gamma$ couplings [3]. In order to perform such tests it is imperative to have precise calculations of hadronic $Z\gamma$ production. Furthermore, the calculations should include the leptonic decay of the Z boson since the Z boson is identified by its leptonic decay products.

At leading order in QCD $[O(\alpha_s^0)]$, hadronic $Z\gamma$ production proceeds via the quark-antiquark annihilation subprocess $q\bar{q} \to Z\gamma$. This process was first calculated in Ref. [4]. $Z\gamma$ events can also be produced at leading order by the photon bremsstrahlung process [5] which proceeds via subprocesses, such as $qg \to Zq$, followed by photon bremsstrahlung from the final state quark. This process becomes significant only at supercollider center-of-mass energies. The production of $Z\gamma$ in association with one or two jets was calculated in Refs. [6] and [7], respectively. The gluon fusion subprocess $gg \to Z\gamma$, which proceeds via a quark box loop, was calculated in Refs. [8,9]. Although this process is of order α_s^2, it can be important at supercollider energies due to the large gluon luminosity; the gluon fusion cross section is 15–30% as large as the $q\bar{q} \to Z\gamma$ Born cross section at supercollider energies [9]. The QCD radiative corrections to hadronic $Z\gamma$ production were calculated in Ref. [10] for the case of a real Z boson in the final state.

In this paper, the calculation in Ref. [10] is extended to include the leptonic decay of the Z boson. Since the Z boson is identified via its leptonic decay products, the inclusion of the leptonic decay in the calculation makes it much more useful for comparing with experimental data. For example, cuts can now be applied to the final state leptons, thus allowing one to more closely mimic the actual experimental conditions.

To date, the Collider Detector at Fermilab (CDF) and D0 experiments at the Fermilab Tevatron collider have collected 12 [11] and 6 [12] $Z\gamma$ events, respectively. Both experiments are expected to collect data corresponding to an integrated luminosity of approximately 100 pb^{-1} by the end of the current collider run (Run 1–B). This represents a fivefold increase in statistics over the presently available data sample. Larger cross sections and luminosities are expected at the CERN Large Hadron Collider (LHC). Thus it should soon be possible to use hadronic $Z\gamma$ production to probe the standard model.

The remainder of this paper is organized as follows. The formalism used in the calculation is briefly reviewed in Sec. II, numerical results for the Tevatron and LHC center-of-mass energies are given in Sec. III, and summary remarks are given in Sec. IV.

II. FORMALISM

The formalism used in the calculation is reviewed in this section. The discussion will be brief since the formalism has already been described in the literature. The calculation is done by using a Monte Carlo method for next-to-leading-order (NLO) calculations [13] in combination with helicity amplitude methods [14]. Details on the NLO calculation of hadronic $Z\gamma$ production for a real Z boson in the final state can be found in Ref. [10] and helicity amplitude calculations of $Z\gamma$ production are described in Ref. [7].

The calculation is done using the narrow-width approximation for the decaying Z boson. This simplifies the calculation greatly for two reasons. First of all, it is possible to ignore Feynman diagrams in which the photon is radiated off one of the final state lepton lines without violating electromagnetic gauge invariance. [Radiative Z decay events can be suppressed by a suitable choice of cuts; see Sec. III B.] Second, in the narrow-width approximation it is particularly easy to extend the NLO calculation of Ref. [10] to include the leptonic decay of the Z boson.

The QCD radiative corrections to hadronic $Z\gamma$ produc-

tion were calculated in Ref. [10] for the case of a real Z boson in the final state. The present calculation extends the results of Ref. [10] to include the leptonic decay of the Z boson. The procedure for incorporating the leptonic decay $Z \to \ell^-\ell^+$ into the NLO calculation of hadronic $Z\gamma$ production is the same as that used in Ref. [15] for incorporating the leptonic decay $W \to \ell\nu$ into a NLO calculation of hadronic $W\gamma$ production. A detailed discussion of the procedure is given in Ref. [15]. Basically, except for the virtual contribution, all the NLO contributions for real $Z\gamma$ production have the form

$$d\sigma^{\rm NLO}(q\bar{q} \to Z\gamma) = d\sigma^{\rm Born}(q\bar{q} \to Z\gamma)\left[1 + C_F\frac{\alpha_s}{2\pi}(\ \dots\ )\right], \quad (1)$$

where $\sigma^{\rm Born}$ is the lowest order Born cross section, $C_F = 4/3$ is the quark-gluon vertex color factor, and α_s is the strong running coupling. Thus the leptonic decays can be incorporated by simply making the replacement

$$d\sigma^{\rm Born}(q\bar{q} \to Z\gamma) \longrightarrow d\sigma^{\rm Born}(q\bar{q} \to Z\gamma \to \ell^-\ell^+\gamma) \quad (2)$$

in the formulas of Ref. [10] for NLO real $Z\gamma$ production.

The simple replacement described in the previous paragraph does not hold for the virtual correction. For this contribution we use the virtual correction for a real on-shell Z boson which we subsequently decay ignoring spin correlations. When spin correlations are ignored, the spin summed squared matrix element for Z boson production and decay factorizes into separate production and decay squared matrix elements: i.e.,

$$\sum_{\rm spins} |\mathcal{M}(q\bar{q} \to Z + X \to \ell\bar{\ell} + X)|^2$$

$$\approx \sum_{\rm spins} \frac{|\mathcal{M}(q\bar{q} \to Z + X)|^2\,|\mathcal{M}(Z \to \ell\bar{\ell})|^2}{(s_{\ell\bar{\ell}} - M_Z^2)^2 + (\Gamma_Z M_Z)^2},$$

$$\approx \sum_{\rm spins} |\mathcal{M}(q\bar{q} \to Z + X)|^2 \times (4\pi)^2\, B(Z \to \ell\bar{\ell})\,\delta(s_{\ell\bar{\ell}} - M_Z^2), \quad (3)$$

where $B(Z \to \ell\bar{\ell})$ is the $Z \to \ell\bar{\ell}$ branching ratio and $s_{\ell\bar{\ell}}$ is the squared $\ell\bar{\ell}$ invariant mass. Neglecting spin correlations slightly modifies the shapes of the angular distributions of the final state leptons, but does not alter the total cross section as long as no angular cuts (e.g., rapidity cuts) are imposed on the final state leptons. For realistic rapidity cuts, cross sections are changed typically by 10% when spin correlations are neglected. Since the size of the finite virtual correction at the hadronic level is only about 1% of the size of the Born cross section, the overall effect of neglecting the spin correlations in the finite virtual correction is to introduce an error of about 0.1%. This is negligible compared to the 20–30% uncertainty from the parton distribution functions and the choice of the scale Q^2. [Note that spin correlations are included everywhere in the calculation except in the virtual contribution.]

III. NUMERICAL RESULTS

Numerical results for NLO $Z\gamma$ production at the Tevatron [$p\bar{p}$ collisions at $\sqrt{s} = 1.8$ TeV] and the LHC [pp collisions at $\sqrt{s} = 14$ TeV] are presented in this section. This section begins with a brief description of the input parameters and acceptance cuts.

A. Input parameters

The numerical results presented in this section were obtained using the two-loop expression for α_s. The QCD scale $\Lambda_{\rm QCD}$ is specified for four flavors of quarks by the choice of the parton distribution functions and is adjusted whenever a heavy quark threshold is crossed so that α_s is a continuous function of Q^2. The heavy quark masses were taken to be $m_b = 5$ GeV and $m_t = 174$ GeV [16]. The standard model parameters used in the numerical simulations are $M_Z = 91.173$ GeV, $M_W = 80.22$ GeV, $\alpha(M_Z) = 1/128$, and $\sin^2\theta_{\rm w} = 1 - (M_W/M_Z)^2$. These values are consistent with recent measurements at the CERN e^+e^- collider LEP [17], the Stanford Linear Collider [18], the CERN Super Proton Synchrotron ($Sp\bar{p}S$ collider [19], and the Fermilab Tevatron collider [20]. The soft and collinear cutoff parameters used in the NLO Monte Carlo formalism (see Ref. [10]) are fixed to $\delta_s = 10^{-2}$ and $\delta_c = 10^{-3}$. The parton subprocesses have been summed over u, d, s, and c quarks. The leptonic branching fractions and the total width of the Z boson are $B(Z \to e^-e^+) = B(Z \to \mu^-\mu^+) = 0.034$ and $\Gamma_Z = 2.487$ GeV, respectively. A single scale $Q^2 = M_{Z\gamma}^2$, where $M_{Z\gamma}$ is the invariant mass of the $Z\gamma$ pair, has been used for the renormalization scale μ^2 and the factorization scale M^2 (see Ref. [10] for a definition of these scales). The numerical results were obtained using the Martin-Roberts-Stirling (MRS) [21] set A parton distribution functions with $\Lambda_4 = 230$ MeV. These distribution functions have been fit to next-to-leading order in the $\overline{\rm MS}$ (modified minimal subtraction) scheme [22], which is the scheme used for the present calculation.

B. Cuts

The cuts imposed in the numerical simulations are motivated by the finite acceptance and resolution of the detector. The finite acceptance of the detector is simulated by cuts on the four-vectors of the final state particles. These cuts include restrictions on the transverse momentum p_T and rapidity y of the photon and leptons.

Since detectors are generally best equipped to measure photons which are isolated, i.e., not accompanied by a large amount of nearby energy [23], a photon isolation cut will be applied in the numerical simulation. First, the leptons and photon are required to be separated in the pseudorapidity-azimuthal-angle plane:

$$\Delta R(\ell,\gamma) = \left[\left(\Delta\phi_{\ell\gamma}\right)^2 + \left(\Delta\eta_{\ell\gamma}\right)^2\right]^{1/2}. \quad (4)$$

A separation cut of $\Delta R(\ell,\gamma) > 0.7$ will be imposed. In

addition, a photon isolation cut typically requires the sum of the hadronic energy $E_{\rm had}$ in a cone of size R_0 about the direction of the photon to be less than a fraction ϵ_h of the photon energy E_γ: i.e.,

$$\sum_{\Delta R<R_0} E_{\rm had} < \epsilon_h E_\gamma \ , \tag{5}$$

with $\Delta R = [(\Delta\phi)^2 + (\Delta\eta)^2]^{1/2}$. A photon isolation cut with $\epsilon_h = 0.15$ [23,24] and $R_0 = 0.7$ will be applied in the numerical results presented in this section. This cut suppresses the portion of the cross section that comes from the photon bremsstrahlung process [5]. The photon bremsstrahlung contribution to $Z\gamma$ production and decay is calculated by convoluting the $O(\alpha_s)$ hard scattering subprocess cross section for Z production and decay with the appropriate parton distribution and fragmentation functions:

$$\sigma_{\rm brem}(AB \to Z\gamma + X) = \sum_{a,b,c} \int G_{a/A}(x_a, M^2)\, G_{b/B}(x_b, M^2)\, D_{\gamma/c}(z_c, M^2) \times d\hat{\sigma}(ab \to Zc \to \ell\bar{\ell}c)\, dx_a\, dx_b\, dz_c \ . \tag{6}$$

Here $G_{a/A}(x_a, M^2)$ is the probability density for finding parton a with momentum fraction x_a in hadron A, $D_{\gamma/c}(z_c, M^2)$ is the probability density for parton c to fragment into a photon with momentum fraction z_c, and M^2 is the factorization scale. When the photon isolation cut described above is included, the range of z is reduced from $0 \le z \le 1$ to $1/(1+\epsilon_h) \le z \le 1$. The LO bremsstrahlung cross section is obtained by using the leading-log parametrizations of the fragmentation functions given in Ref. [25]. At next-to-leading order there are collinear singularities associated with the final state bremsstrahlung which must be factorized and absorbed into the fragmentation functions. The NLO modifications to the fragmentation functions can be found in Ref. [10]. The suppression of the photon bremsstrahlung contribution by the photon isolation cut is beneficial since the fragmentation functions are not well known.

Before summarizing the cuts, it is useful to discuss cuts which will suppress radiative Z decays. Since photon radiation from the final state lepton lines is ignored in the calculation, it is necessary to impose cuts which will efficiently suppress contributions from these diagrams. In radiative Z decays the lepton-photon separation in ΔR space peaks sharply at small values due to the collinear singularity associated with the diagrams in which the photon is radiated from a final state lepton line. A separation cut on $\Delta R(\ell, \gamma)$, which has already been adopted, will therefore suppress radiative Z decay events. Contributions from radiative Z decay can be further reduced by a cut on the $\ell^-\ell^+\gamma$ invariant mass. In radiative Z decays the $\ell^-\ell^+\gamma$ system has an invariant mass $M(\ell^-\ell^+\gamma)$ close to M_Z, whereas for $Z\gamma$ production $M(\ell^-\ell^+\gamma)$ is always larger than M_Z if finite Z-width effects are ignored. Thus $\ell^-\ell^+\gamma$ events originating from radiative Z decays can be suppressed if $M(\ell^-\ell^+\gamma)$ is required to be slightly above M_Z. Note that this requirement is automatically satisfied in the present calculation since putting the Z boson on the mass shell and demanding the photon to have $p_T(\gamma) > p_T^{\rm min}$ requires that

$$M(\ell^-\ell^+\gamma) > p_T^{\rm min} + \left[M_Z^2 + (p_T^{\rm min})^2\right]^{1/2} \ . \tag{7}$$

Thus no additional cuts are needed in the numerical simulation to suppress the radiative Z decays.

The complete set of cuts can now be summarized as follows:

Tevatron	LHC
$p_T(\gamma) > 10$ GeV	$p_T(\gamma) > 50$ GeV
$p_T(\ell) > 20$ GeV	$p_T(\ell) > 25$ GeV
$\lvert y(\gamma)\rvert < 1.0$	$\lvert y(\gamma)\rvert < 2.5$
$\lvert y(\ell)\rvert < 2.5$	$\lvert y(\ell)\rvert < 3.0$
$\Delta R(\ell, \gamma) > 0.7$	$\Delta R(\ell, \gamma) > 0.7$
$\sum_{\Delta R<0.7} E_h < 0.15\, E_\gamma$	$\sum_{\Delta R<0.7} E_h < 0.15\, E_\gamma$

C. Cross sections

The total LO and NLO cross sections for the process $p\overset{(-)}{p} \to Z\gamma + X \to \ell^-\ell^+\gamma + X$ are given in Table I for center-of-mass energies corresponding to the present Tevatron [$\sqrt{s} = 1.8$ TeV], an upgraded Tevatron [$\sqrt{s} = 3.5$ TeV], and the proposed LHC [$\sqrt{s} = 14$ TeV]. The cross sections in Table I have been summed over $\ell = e, \mu$ and include the cuts listed in Sec. III B. Note that the LHC cross sections are smaller than the Tevatron cross sections due to the more restrictive p_T cuts used for the LHC case [in particular the $p_T(\gamma)$ cut].

The differential cross sections presented here have also been summed over $\ell = e, \mu$ and include the cuts listed in Sec. III B. The figures are arranged in two parts, with parts (a) and (b) being the results for the Tevatron [$\sqrt{s} = 1.8$ TeV] and LHC [$\sqrt{s} = 14$ TeV] energies, respectively. NLO and LO results are shown with solid and dashed lines, respectively.

Figure 1 shows the distribution of the invariant mass of the $\ell^-\ell^+\gamma$ system $M(\ell^-\ell^+\gamma)$. The NLO corrections are fairly uniform in the invariant mass, so that the NLO distribution can be approximately described by simply scaling up the LO distribution by a factor of 1.2 (1.3) at the Tevatron (LHC). The NLO corrections are larger

TABLE I. Total LO and NLO cross sections for the process $p\overset{(-)}{p} \to Z\gamma + X \to \ell^-\ell^+\gamma + X$, for center-of-mass energies corresponding to the present Tevatron [$\sqrt{s} = 1.8$ TeV], an upgraded Tevatron [$\sqrt{s} = 3.5$ TeV], and the proposed LHC [$\sqrt{s} = 14$ TeV]. The cross sections have been summed over $\ell = e, \mu$ and the cuts listed in Sec. III B have been imposed.

$\sqrt{s}$ (TeV)	$p\overset{(-)}{p}$		σ (fb)
1.8	$p\bar{p}$	LO	360
		NLO	420
3.5	$p\bar{p}$	LO	540
		NLO	620
14	pp	LO	230
		NLO	310

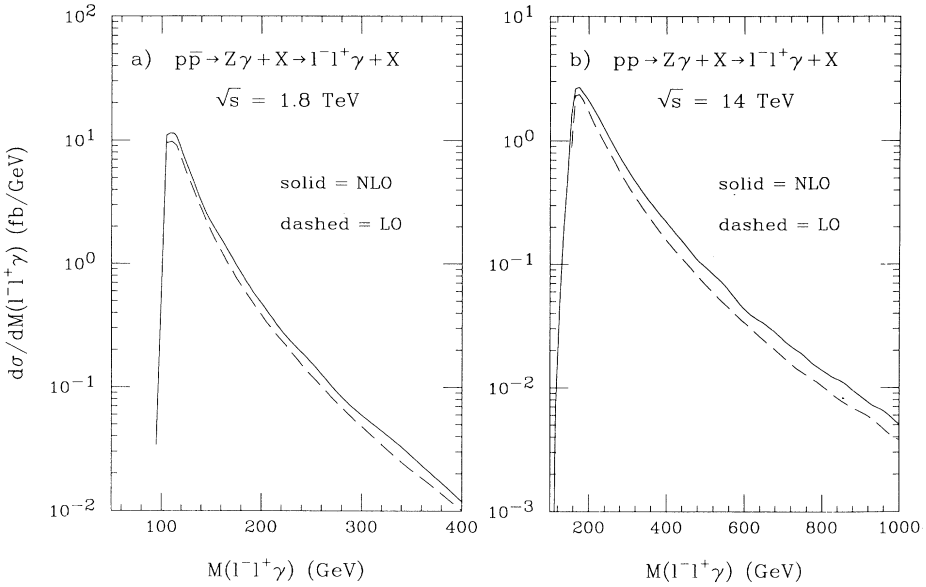

FIG. 1. Invariant mass distribution of the $\ell^-\ell^+\gamma$ system for the process $p\bar{p}^{(-)} \to Z\gamma + X \to \ell^-\ell^+\gamma + X$. Parts (a) and (b) are for the Tevatron and LHC center-of-mass energies, respectively. The NLO (solid line) and LO (dashed line) cross sections are shown. The cross sections have been summed over $\ell = e, \mu$ and the cuts listed in Sec. III B have been imposed.

at the LHC due to the larger gluon density at the LHC energy.

The rapidity distributions [in the laboratory frame] for the charged leptons $y(\ell)$ and the Z boson $y(Z)$ are shown in Figs. 2 and 3, respectively. [Both leptons have been histogrammed in Fig. 2.] The NLO corrections are largest in the central rapidity region where the cross section is also the largest; however, the NLO cross section is uniformly enhanced over the LO cross section in the entire rapidity range. This fact is illustrated in Fig. 4 where the ratio of the NLO to LO cross section is plotted as a function of $y(\ell)$. The ratio has a constant value of 1.2 (1.3) at the Tevatron (LHC) center-of-mass energy.

The angular distributions of the leptonic decay products contain information on the helicity of the Z boson and are simplest in the rest frame of the Z boson. Figure 5 shows the polar angle distribution of the ℓ^- in the Z boson rest frame, measured with respect to the Z boson direction in the $Z\gamma$ rest frame, i.e., $\cos\theta_- = \hat{p}_{\ell^-} \cdot \hat{p}_Z$ where $\hat{p}_{\ell^-}$ is the unit-normalized three-momentum of the ℓ^- in the Z boson rest frame and $\hat{p}_Z$ is the unit-normalized three-momentum of the Z boson in the $Z\gamma$ rest frame. If no cuts were imposed on the leptons, this distribution would exhibit a $1 + \cos^2\theta_-$ dependence, which is indicative of transversely polarized Z bosons. Unfortunately, the shapes of the distributions in Fig. 5 indicate that there is little or no polarization information left in the distributions. In the presence of cuts, the angular distribution of leptons produced via the decay of a gauge boson is, in general, dominated by kinematic effects rather than

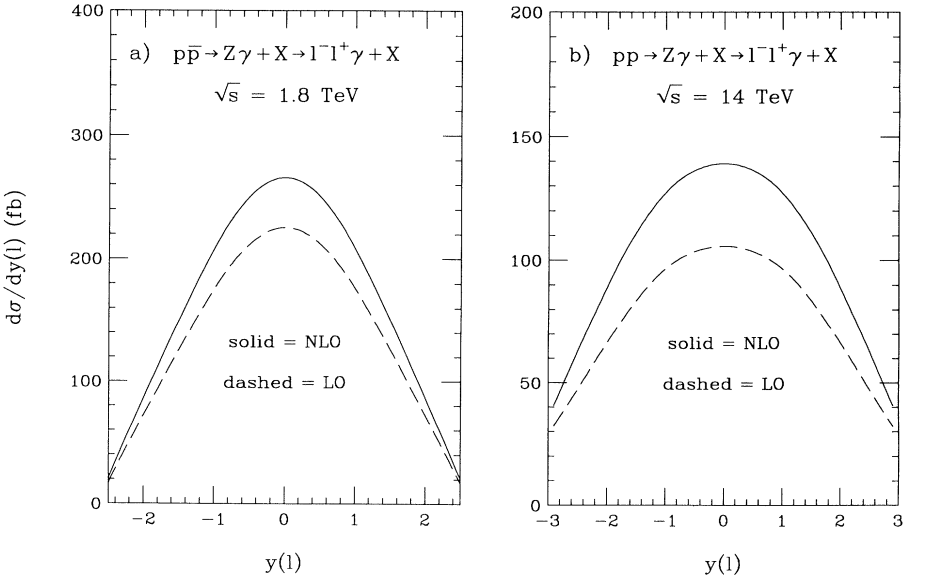

FIG. 2. Same as Fig. 1 but for the rapidity distribution of the leptons.

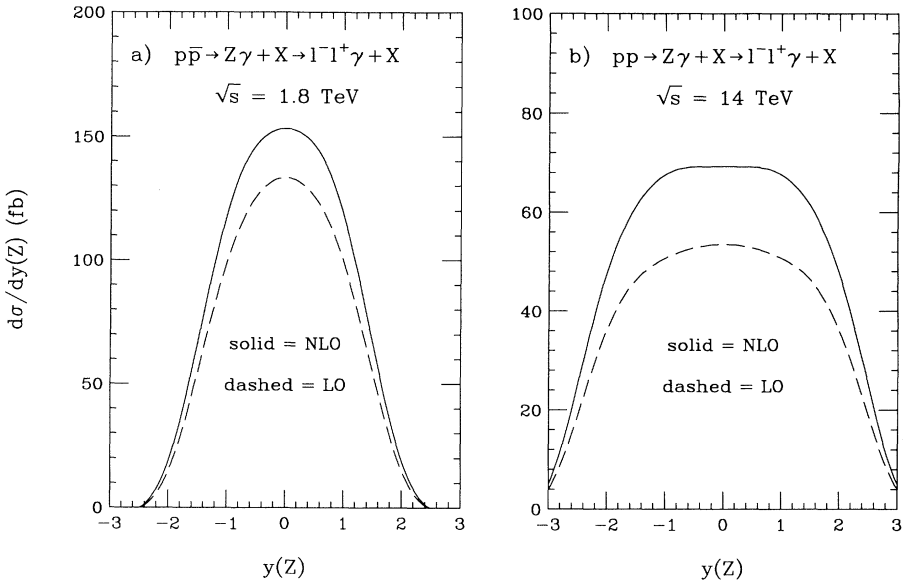

FIG. 3. Same as Fig. 1 but for the rapidity distribution of the Z boson.

polarization effects [26]. The sharp drops in the distributions near $\cos\theta_- = \pm 1$ are due to the kinematic cuts. The NLO corrections are once again uniform over the range of $\cos\theta_-$.

In the distributions presented so far, the NLO corrections simply enhanced the LO distributions and produced little or no change in the shapes of the distributions. This is not the case for transverse momentum distributions; instead, the NLO corrections increase with the transverse momentum. The transverse momentum distributions of the charged leptons $p_T(\ell)$, the Z boson $p_T(Z)$, and the photon $p_T(\gamma)$, are shown in Figs. 6, 7, and 8, respectively. [Both leptons have been histogrammed in Fig. 6.] In all three figures, the NLO corrections increase as the transverse momentum increases. The large corrections at high p_T are due to the contributions from the real emission subprocesses $q\bar{q} \to Z\gamma g$, $qg \to Z\gamma q$, and $g\bar{q} \to Z\gamma\bar{q}$ which enter at order α_s.

Comparing the curves in Fig. 6 for the two different energies, one sees that the curves at the LHC energy do not turn over at small values of $p_T(\ell)$. This is simply due to the more restrictive cuts used for the LHC case.

The NLO and LO $p_T(Z)$ distributions in Fig. 7 have different behaviors at small values of $p_T(Z)$. At LO the Z boson and photon are back-to-back in the plane transverse to the beam direction, thus the $p_T(Z)$ distribution cuts off at the value of the minimum $p_T(\gamma)$ cut [$p_T(\gamma) = 10$ (50) GeV for the Tevatron (LHC)]. The NLO cross section, on the other hand, has a finite but rapidly decreasing distribution for values of $p_T(Z)$ below

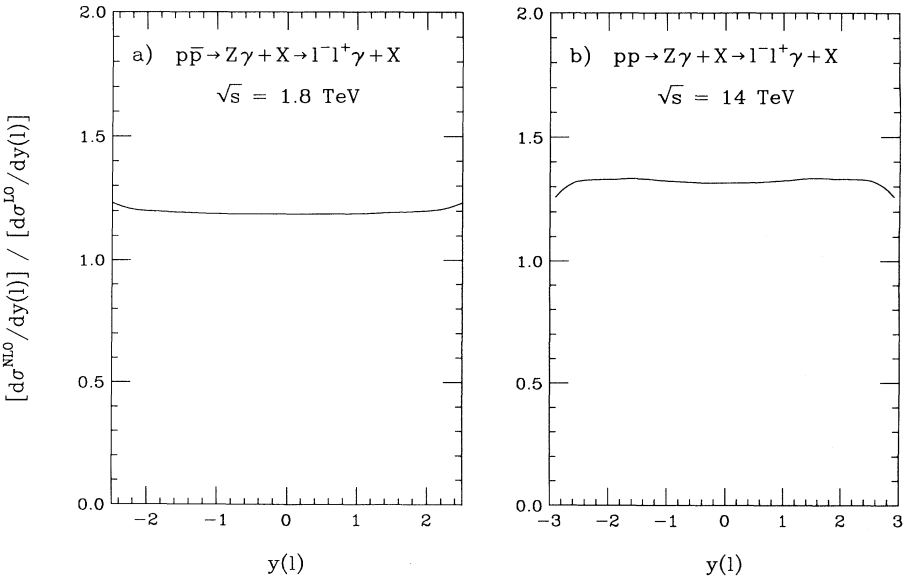

FIG. 4. The ratio $[d\sigma^{\rm NLO}/dy(\ell)]/[d\sigma^{\rm LO}/dy(\ell)]$ plotted vs $y(\ell)$ for the process $p\overset{(-)}{p} \to Z\gamma + X \to \ell^-\ell^+\gamma + X$. Parts (a) and (b) are for the Tevatron and LHC center-of-mass energies, respectively. The cuts listed in Sec. III B have been imposed.

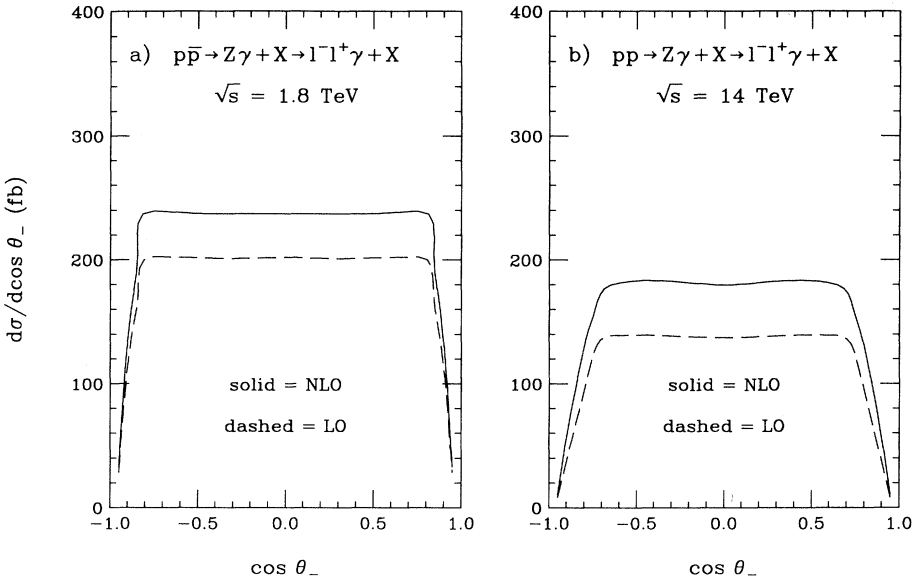

FIG. 5. Same as Fig. 1 but for the angular distribution of the negatively charged lepton. The angle θ_- is measured in the Z boson rest frame with respect to the Z boson direction in the $Z\gamma$ rest frame.

the minimum $p_T(\gamma)$ cut. In this region of small $p_T(Z)$, the photon is recoiling against a jet.

In addition to showing the NLO and LO differential cross sections vs $p_T(\gamma)$, Fig. 8 also shows the 0-jet and 1-jet components of the NLO inclusive cross section. Here a jet is defined as a final state quark or gluon with

$$p_T(j) > 10 \text{ GeV} \qquad \text{and} \qquad |y(j)| < 2.5 \qquad (8)$$

at the Tevatron, and

$$p_T(j) > 50 \text{ GeV} \qquad \text{and} \qquad |y(j)| < 3 \qquad (9)$$

at the LHC. The sum of the 0-jet and 1-jet cross sections is equal to the inclusive NLO cross section. The decomposition shows that the 1-jet component is small at the Tevatron energy, and is small at low values of $p_T(\gamma)$ but becomes the dominant component at large values of $p_T(\gamma)$ at the LHC energy. Thus most of the NLO corrections at high $p_T(\gamma)$ are due to events with hard jets. This is also true for the $p_T(\ell)$ and $p_T(Z)$ distributions.

The increase of the NLO corrections with the transverse momentum is clearly illustrated in Fig. 9 where the ratio of the NLO to LO cross section is plotted as a function of $p_T(\gamma)$. The ratio increases from 1.2 to 1.5 (1.3 to 2.0) over the range of $p_T(\gamma)$ shown for the Tevatron (LHC) center-of-mass energy.

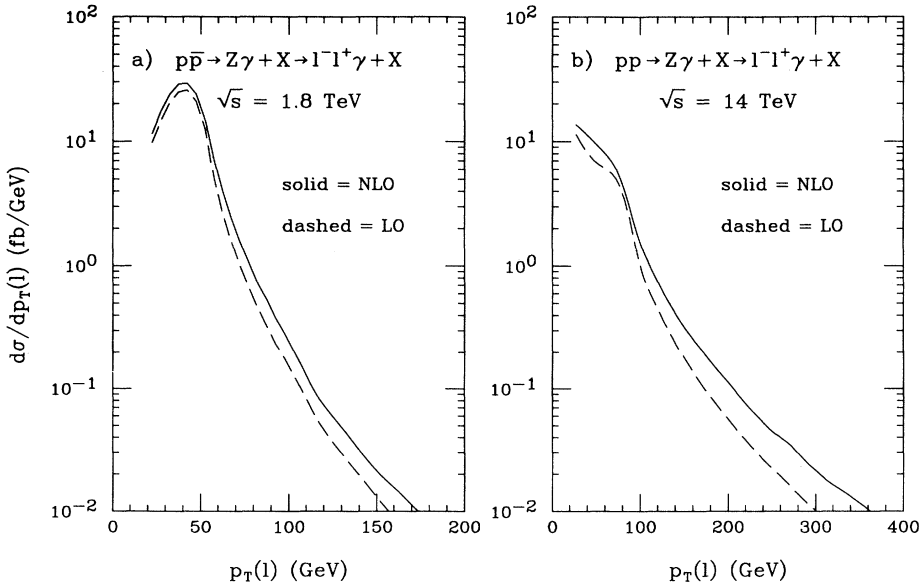

FIG. 6. Same as Fig. 1 but for the transverse momentum distribution of the charged leptons.

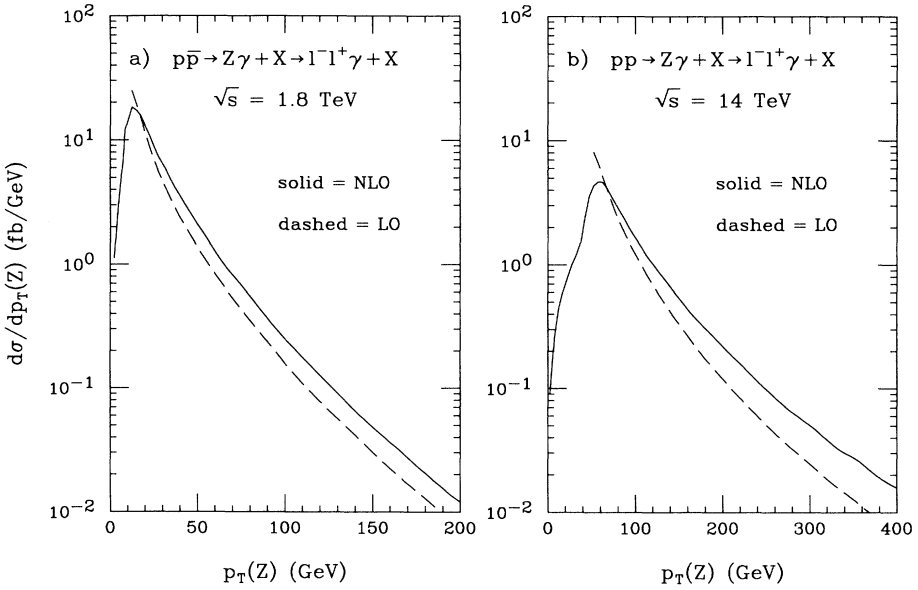

FIG. 7. Same as Fig. 1 but for the transverse momentum distribution of the Z boson.

IV. SUMMARY

The QCD radiative corrections to hadronic $Z\gamma$ production have been calculated to order α_s with leptonic decays of the Z boson included. The inclusion of the leptonic decays makes the calculation more realistic since it is the leptonic decay products that are observed in an experiment. Distributions of the final state decay products have been given for the Tevatron and LHC center-of-mass energies. The calculation includes typical acceptance cuts on the final state leptons and photon.

The calculation is done by using the Monte Carlo method for NLO calculations in combination with helicity amplitude methods. With the Monte Carlo method it is easy to impose experimentally motivated acceptance cuts on the final state particles; also, it is possible to calculate the order α_s QCD corrections for exclusive channels, e.g., $p\overset{(-)}{p} \to Z\gamma + 0$ jet. The narrow-width approximation has been used for the decaying Z boson. This simplifies the calculation greatly since it is possible to ignore contributions from radiative decay diagrams without violating electromagnetic gauge invariance. Furthermore, in the narrow-width approximation it is particularly easy to extend the NLO calculation of real $Z\gamma$ production to include the leptonic decay of the Z boson. Spin correlations are included everywhere in the calculation except in the virtual contribution where they can be safely neglected.

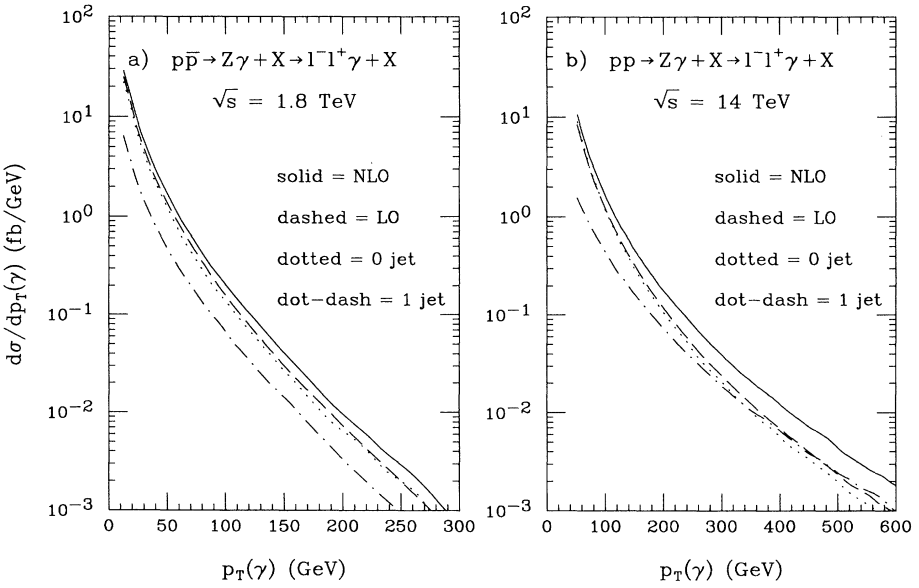

FIG. 8. Same as Fig. 1 but for the transverse momentum distribution of the photon. In addition, the 0-jet (dotted line) and 1-jet (dot-dashed line) cross sections are also shown.

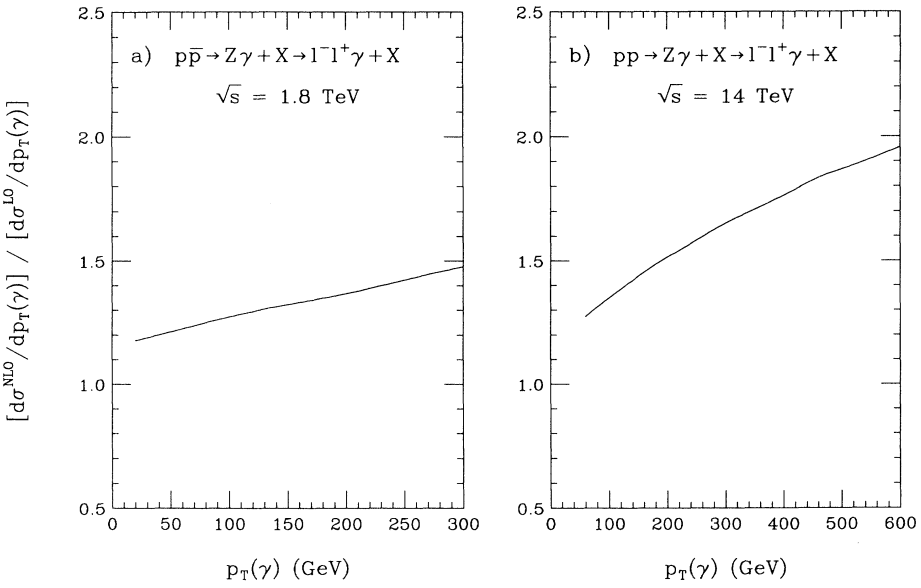

FIG. 9. The ratio $[d\sigma^{\rm NLO}/dp_T(\gamma)]/[d\sigma^{\rm LO}/dp_T(\gamma)]$ plotted vs $p_T(\gamma)$ for the process $p\overset{(-)}{p} \to Z\gamma + X \to \ell^-\ell^+\gamma + X$. Parts (a) and (b) are for the Tevatron and LHC center-of-mass energies, respectively. The cuts listed in Sec. III B have been imposed.

In general, the QCD radiative corrections are uniform in invariant mass and angular distributions; these distributions are scaled up in magnitude by the corrections, but undergo little change in shape. In contrast, the QCD radiative corrections increase with transverse momentum, and as a result, the p_T distributions are significantly enhanced at high p_T. The large corrections at high p_T are due to contributions from the real emission processes which enter at order α_s. The QCD radiative corrections increase with the center-of-mass energy due to the increasing gluon density in the proton. These behaviors of the NLO corrections are qualitatively the same as those found in the NLO corrections to $W^{\pm}\gamma$ [15], ZZ, W^-W^+, and $W^{\pm}Z$ production [27].

ACKNOWLEDGMENTS

Discussions with T. Diehl, S. Errede, and T. Muller regarding the status of $Z\gamma$ production at the Tevatron are gratefully acknowledged. This work has been supported in part by Department of Energy Grant No. DE-FG03-91ER40674 and by Texas National Research Laboratory Grant No. RGFY93-330.

[1] E. Eichten, I. Hinchliffe, K. Lane, and C. Quigg, Rev. Mod. Phys. **56**, 579 (1984); **58**, 1065(E) (1986).
[2] M. Leurer, H. Harari, and R. Barbieri, Phys. Lett. **141B**, 455 (1985).
[3] U. Baur and E. L. Berger, Phys. Rev. D **47**, 4889 (1993); Z. Ryzak, Nucl. Phys. **B289**, 301 (1987); H. Baer, V. Barger, and K. Hagiwara, Phys. Rev. D **30**, 1513 (1984).
[4] F. Renard, Nucl. Phys. **B196**, 93 (1982).
[5] J. Ohnemus and W. J. Stirling, Phys. Lett. B **298**, 230 (1993).
[6] U. Baur, E. W. N. Glover, and J. J. van der Bij, Nucl. Phys. **B318**, 106 (1989).
[7] V. Barger, T. Han, J. Ohnemus, and D. Zeppenfeld, Phys. Rev. D **41**, 2782 (1990).
[8] Ll. Ametller, E. Gava, N. Paver, and D. Treleani, Phys. Rev. D **32**, 1699 (1985).
[9] J. J. van der Bij and E. W. N. Glover, Phys. Lett. B **206**, 701 (1988).
[10] J. Ohnemus, Phys. Rev. D **47**, 940 (1993).
[11] CDF Collaboration, F. Abe *et al.*, Phys. Rev. Lett. (to be published); S. Errede, in Proceedings of the 27th International Conference on High Energy Physics, Glasgow, Scotland, 1994 (unpublished); S. Errede, FERMILAB-CONF-94/158-E.
[12] D0 Collaboration, J. Ellison, in Proceedings of the 1994 DPF Meeting, Albuquerque, New Mexico (unpublished).
[13] J. Ohnemus and J. F. Owens, Phys. Rev. D **43**, 3626 (1991); J. Ohnemus, *ibid.* **44**, 1403 (1991); **44**, 3477 (1991); H. Baer, J. Ohnemus, and J. F. Owens, *ibid.* **40**, 2844 (1989); **42**, 61 (1990); Phys. Lett. B **234**, 127 (1990); H. Baer and M. H. Reno, Phys. Rev. D **43**, 2892 (1991); B. Bailey, J. Ohnemus, and J. F. Owens, *ibid.* **46**, 2018 (1992); J. Ohnemus and W. J. Stirling, *ibid.* **47**, 2722 (1993); H. Baer, B. Bailey, and J. F. Owens, *ibid.* **47**, 2730 (1993); L. Bergmann, Ph.D. dissertation, Florida State University, 1989.
[14] P. De Causmaecker, R. Gastmans, W. Troost, and T. T. Wu, Phys. Lett. **105B**, 215 (1981); Nucl. Phys. **B206**, 53 (1982); F. A. Berends, R. Kleiss, P. De Causmaecker, R. Gastmans, W. Troost, and T. T. Wu, *ibid.* **B206**, 61 (1982); CALKUL Collaboration, F. A. Berends *et al.*, *ibid.* **B239**, 382 (1984); K. Hagiwara and D. Zeppenfeld, *ibid.* **B274**, 1 (1986); Z. Xu, D.-H. Zhang, and L. Chang, *ibid.* **B291**, 392 (1987); R. Gastmans and T. T. Wu, *The Ubiquitous Photon: Helicity Method for QED and QCD* (Oxford University Press, Oxford, 1990).
[15] U. Baur, T. Han, and J. Ohnemus, Phys. Rev. D **48**, 5140 (1993).
[16] CDF Collaboration, F. Abe *et al.*, Phys. Rev. Lett. **73**,

225 (1994); Phys. Rev. D **50**, 2966 (1994).
[17] LEP Collaborations: ALEPH, DELPHI, L3, OPAL, and the LEP Electroweak Working Group, "Updated Parameters of the Z^0 Resonance from Combined Preliminary Data of the LEP Experiments," Report No. CERN/PPE/93-157 (unpublished); Phys. Lett. B **276**, 247 (1992).
[18] SLD Collaboration, K. Abe *et al.*, Phys. Rev. Lett. **73**, 25 (1994).
[19] UA2 Collaboration, J. Alitti *et al.*, Phys. Lett. B **241**, 150 (1990); UA1 Collaboration, G. Arnison *et al.*, Europhys. Lett. **1**, 327 (1986).
[20] CDF Collaboration, F. Abe *et al.*, Phys. Rev. Lett. **65**, 2243 (1990); Phys. Rev. D **43**, 2070 (1991); D0 Collaboration, N. A. Graf, Report No. FERMILAB-CONF-94-021-E (unpublished); Q. Zhu *et al.*, Report No. FERMILAB-CONF-93-396-E (unpublished).
[21] A. D. Martin, R. G. Roberts, and W. J. Stirling, Phys. Rev. D **50**, 6734 (1994).
[22] W. A. Bardeen, A. J. Buras, D. W. Duke, and T. Muta, Phys. Rev. D **18**, 3998 (1978).
[23] CDF Collaboration, F. Abe *et al.*, Phys. Rev. Lett. **68**, 2734 (1992); Phys. Rev. D **48**, 2998 (1993).
[24] P. Aurenche, R. Baier, and M. Fontannaz, Phys. Rev. D **42**, 1440 (1990); P. Aurenche *et al.*, in *Proceedings of the ECFA Large Hadron Collider Workshop*, Aachen, Germany, 1990, edited by G. Jarlskog and D. Rein (CERN Report No. 90-10, Geneva, Switzerland, 1990), Vol. II, p. 69.
[25] D. W. Duke and J. F. Owens, Phys. Rev. D **26**, 1600 (1982).
[26] E. Mirkes and J. Ohnemus, Phys. Rev. D **50**, 5692 (1994).
[27] J. Ohnemus, Phys. Rev. D **50**, 1931 (1994).